frontiers | Frontiers in Earth Science

TYPE Original Research
PUBLISHED 29 December 2023
DOI 10.3389/feart.2023.1330766

OPEN ACCESS

EDITED BY
Junrong Zhang,
China University of Geosciences Wuhan, China

REVIEWED BY
Lishuai Jiang,
Shandong University of Science and Technology, China
Geng Jiabo,
Jiangxi University of Science and Technology, China
Gaili Xue,
Taiyuan University of Technology, China

*CORRESPONDENCE
Lijie Guo,
guolijie@bgrimm.com

RECEIVED 31 October 2023
ACCEPTED 20 November 2023
PUBLISHED 29 December 2023

CITATION
Zheng D, Liu G, Guo L, Yang X, Wu S and Zhao Y (2023), Initial pore distribution characteristics and crack failure development of cemented tailings backfill under low impact amplitude. *Front. Earth Sci.* 11:1330766. doi: 10.3389/feart.2023.1330766

Initial pore distribution characteristics and crack failure development of cemented tailings backfill under low impact amplitude

Di Zheng[1,2], Guangsheng Liu[1,2], Lijie Guo[1,2]*, Xiaocong Yang[1,2], Shan Wu[1,2] and Yue Zhao[1,2]

[1]Beijing General Research Institute of Ming and Metallurgy, Beijing, China, [2]National Centre for International Research on Green Metal Mining, Beijing, China

The stability of the cemented paste backfill is threatened by the dynamic disturbance during the excavation of the surrounding ore body. In this paper, the computerized tomography (CT) and Split Hopkinson Pressure Bar (SHPB) tests were conducted to explore the initial pore distribution characteristics of the cemented tailings backfill (CTB) and the development of the crack under low impact amplitude. SHPB tests were conducted with impact amplitudes of 34, 37, and 39 mV, respectively. Results show that the initial pores of CTB were steadily distributed with the height of CTB. The CTB contained many initial pores with similar pore size distribution characteristics, and the largest number of pores is between 0.1 and 0.3 mm. Most of the cracks in CTB after low impact amplitude develop and expand along the initial pores, and the damage of CTB mainly exists in shear cracks. A dependence has been established that the dynamic uniaxial compressive strength of the CTB increases, the total crack volume first increases and then decreases, and the number of cracks increases as the impact amplitude increases. The research results can provide a valuable reference for the dynamic performance of CTB under low impact amplitude and the design of mining backfill.

KEYWORDS

cemented tailings backfill, initial pore, 3D visualization, Split Hopkinson pressure bar tests, pore distribution characteristic, crack volume

1 Introduction

As the primary ore body and associated waste rock are extracted during the mining process, underground spaces of varying sizes are formed. Under the influence of gravity, unbalanced ground stress, and other factors, ground cracks first occur in the goaf area and gradually develop into ground collapse in the goaf. Geological disasters reduce the environmental quality and endanger human safety directly or indirectly (Dong et al., 2023; Wu et al., 2023). Mine backfill can control the occurrence of such geological disasters, so it has been widely used in underground metal ore mining. Mine backfill has prevented and controlled geohazards and has been widely used in underground metal ore extraction (Guo et al., 2022; Guggari et al., 2023).

The cured backfill, also known as cemented tailings backfill (CTB), serves as a support structure or working platform for the excavated stopes (Zhu et al., 2016; Lu et al., 2018), effectively controlling mining pressure (Mohanto and Deb, 2020), reducing mineral losses by pillars extraction, reducing ground surface subsidence and protecting buildings on the surface, improving the safety of mining operations (Deng et al., 2022), reducing the cost of mining and minimize the load on the environment (Solismaa et al., 2021). It could effectively utilize environmentally destructive tailings produced after mineral processing, mitigating the economic and environmental hazards caused by mine tailings disposal (Kasap et al., 2022; Xue and Yilmaz, 2022).

There are many different mining methods with backfill in underground metal mines, but long-hole open stoping with delayed backfill mining is widely used worldwide (Emad et al., 2014; Wang et al., 2021). First, the primary stopes are mined, and the CTB fills the mined voids. The CTB plays the role of artificial vertical pillars (Sun et al., 2018; Liu et al., 2019). In actual mine production, blasting occurs in the ore, and the CTB is often damaged by medium and long-distance ore blasting with low power disturbance strength (Onederra et al., 2013; Li et al., 2022).

The dynamic compressive strength of CTB is usually obtained by performing the Split Hopkinson Pressure Bar (SHPB) tests on CTB samples (Zhang et al., 2017; Sun et al., 2022). Many experiments have shown that CTB materials' mechanical behavior differs at different strain rates. Cao carried out the SHPB tests considering different loading rates and quantitatively investigated the relationship between uniaxial compressive strength (UCS) and dynamic characteristics of backfill (Cao et al., 2020). Tan studied the dynamic strength and deformation characteristics of CTB samples under multiple cyclic impacts by the SHPB test (Tan et al., 2019). Most of the studies are about the dynamic compressive strength of the CTB at medium to high strain rates (Chen et al., 2021; Xue et al., 2021), and there are few studies on low strain rate impact tests. The CTB is also subject to medium and long-range blasting damage in actual production, and the dynamic disturbance strength is low. The CTB's stability directly affects the mine's safe recovery and the loss depletion rate of mineral resources (Du et al., 2022; Xia et al., 2023), so the CTB mechanical properties under low dynamic disturbance are widely concerned.

The CTB is a composite material. Even though the macroscopic performance is homogeneous, the internal structure of the CTB is bound to have initial defects, such as pores (Sarkar and Siddiqua, 2016; Zheng et al., 2022), due to the uneven distribution of the tailing particle size and hydration products (Wang J. et al., 2022). These initial defects are closely related to the CTB mechanical properties, and studying detailed initial defects helps us deepen our understanding of CTB (Wang et al., 2019; Jafari et al., 2021). Liu et al. believed that the UCS of cemented paste backfill using sulfide tailings is negatively correlated with pores (Liu et al., 2020). Zhang et al. found that due to the bonding effect of hydration products, the UCS of cemented paste backfill (CPB) increases, and there is an exponential relationship between the porosity and UCS (Zhang et al., 2022; 2023). Tian et al. supposed that higher cumulative pore volume and coarser pore structure are associated with a lower strength of the CPB samples (Tian and Fall, 2021).

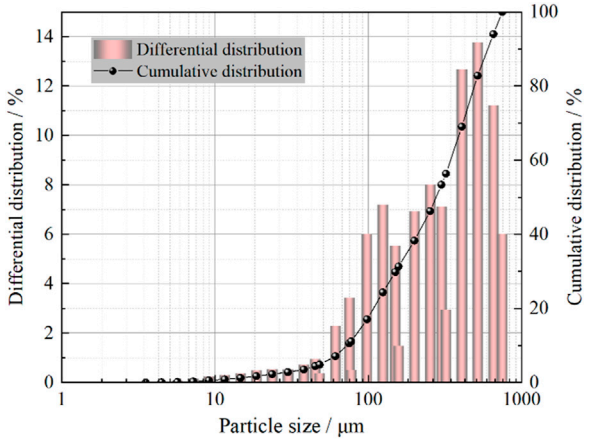

FIGURE 1
Particle size distribution of tailings.

Consequently, the pore structure of cementitious structures should be determined truthfully. As an emerging nondestructive testing method, the computerized tomography (CT) technique has been applied by many scholars for the pore analysis of CTB (Sun et al., 2017; Huang et al., 2023). The polarized and fluorescent microscopy technique is also a direct method to analyze the microcracks (Ghasemi et al., 2020). Wang observed that the fracture development changes from rich to single through the fracture morphology and CT image analysis of fiber reinforced cemented tailings backfill samples with different height-to-diameter ratios (Wang A. et al., 2022). Li found that connected pores and microcracks are prone to develop as cracks under the action of external loads (Li et al., 2021; Li et al., 2023).

Analyzing the above, it can be noted that crack failure development of CTB under low impact amplitude is a topical issue. Therefore, this study aims to reveal initial pore distribution characteristics and crack failure development of CTB to achieve this. It is necessary to solve the following tasks: 1) The CTB was carried out by CT test and visualized by 3D reconstruction technique; 2) The CTB's mesoscopic parameters such as porosity and pore size are also analyzed; 3) The SHPB test with low impact amplitude was carried out to compare the crack development of CTB.

2 Materials and methods

2.1 Materials

The density of the gold tailings used in the test is 2.34 g/cm^3, and the specific surface area by weight is 39.595 m^2/kg. The wet tailings were initially oven dried before the test, and then the particle size was analyzed by an LS-POP laser particle size analyzer. Figure 1 shows the particle size distribution curve of the tailings. The d_{50} of the tailings is 321.3 μm, classified as coarse tailings according to the tailings distribution and the nonuniform coefficient of the particle size composition of the tailings is 5. A chemical composition analysis of tailings was carried out, and the analysis results are shown in

TABLE 1 Chemical composition of tailings.

Component	SiO_2	Al_2O_3	K_2O	CaO	Fe_2O_3	SO_3	MnO	MgO	Au
Content (%)	58.40	7.03	4.02	2.08	1.29	0.70	0.04	<0.15	<0.01

TABLE 2 Chemical composition of 42.5 M ordinary Portland cement.

Component	CaO	SiO2	SO3	Al2O3	Fe2O3	TiO2	K2O	MnO
Content (%)	35.40	17.10	3.21	2.39	2.19	0.56	0.44	0.10

FIGURE 2
The prepared CTB samples.

Table 1. The chemical composition of the tailings was tested by a sequential X-ray fluorescence spectrometer (brand: German SPECTRO, model: XSORT BT). The main components of the tailings are SiO_2, accounting for 58.4%, Al_2O_3, 7.03%, K_2O and CaO, 4.02%, and 2.08%, respectively.

The cementitious material was selected as 42.5 M ordinary Portland cement, in which the active ingredient CaO accounted for 35.4 wt%, followed by SiO_2 accounting for 17.1%. The cementitious material was selected as 42.5 M ordinary Portland cement, and the chemical composition was analyzed as shown in Table 2, in which the active ingredient CaO accounted for 35.4 wt%, followed by SiO_2 accounting for 17.1%.

2.2 Sample preparation

The CTB samples possess a slurry content of 75 wt% and a cement tailings ratio of 1:4. The experimental personnel used a standard electronic scale to weigh 138 g tailings with the requirements

of ASTM C192/C192 M (Gerges et al., 2015), 34.5 g cement, and 57.5 g water and thoroughly stirred the materials in the mixer for 180 s. Then, the stirred slurry was poured into the cylindrical mold (the mold with a height of 50 mm and a diameter of 50 mm). After 48 h, the samples were demolished from the mold first and then returned to the curing box (20°C ± 1°C in temperature, 90% ± 1% in humidity) until 28 days (Zheng et al., 2021). After 28 days, the sample was gently polished at both ends to meet the flatness requirements of the dynamic load test. Figure 2 shows the prepared CTB specimen.

2.3 Experimental equipment

2.3.1 SHPB test

The SHPB test equipment, as show in Figure 3, comprises a nitrogen cylinder, emission chamber, impact bar, incident bar, transmitted bar, absorption device, ultra-dynamic strain gauge, timer, oscilloscope, and computer. The material of the bar in the SHPB test equipment is 40Cr alloy steel, with a density of 7800 kg/m^3, wave speed of 5200 m/s, and diameter of 50 mm. The impact, incident and transmitted bar lengths are 0.4 m, 1.5 m, and 1.5 m, respectively. It should be noted that before the start of the test, two strain gauges of the type BX120-2AA need to be pasted at middle positions on both sides of the incident bar and transmitted bar, respectively. The resistance value of the strain gauge used is 120 ± 0.2Ω, and the sensitivity coefficient is 2.11% ± 1%. Four strain gauges are connected to the ultra-dynamic strain gauge through some wires and a strain bridge box.

2.3.2 Computerized tomography

This paper's X-ray computerized tomography (CT) testing system is German YXLON high-resolution testing equipment. This system is a "double source double probe," "double source" is 225kV and 450 kV light source, and "double probe" is a flat panel and line array detector. This experiment used a 225 kV micro-CT system and continuous rotation scanning. A voxel resolution of 68 μm was achieved.

2.4 Method

2.4.1 3D visualization

The two-dimensional (2D) tomographic images obtained cannot visually express the initial pore and crack development of the three-dimensional (3D) structure of the CTB (Fang et al., 2023). They can only understand the distribution information of minerals, pores, and cracks in a certain section of the CTB. Therefore, a series of 2D CT data scanned from the specimen needs to be transformed into 3D stereo images to observe the fine internal structure of the CTB visually. The 3D visualization of 2D cross-sections of the CTB is shown in Figure 4.

The 3D visualization is to superimpose a series of acquired CT slice image data, as in Figure 4A, and convert them into 3D data,

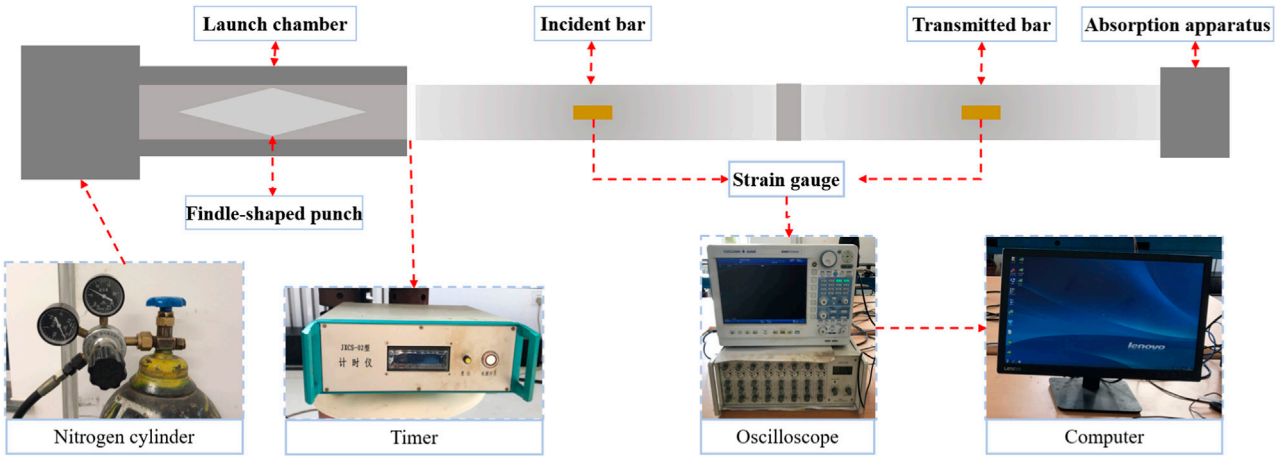

FIGURE 3
Diagram of SHPB test equipment.

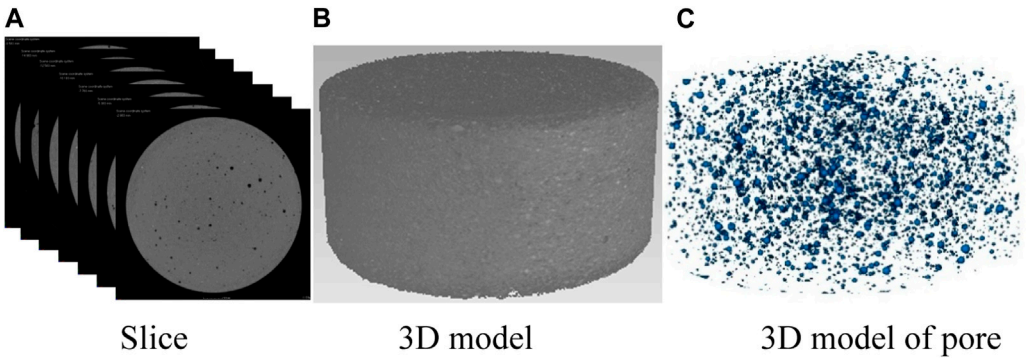

FIGURE 4
3D visualization of 2D cross-sections of the CTB.

Figure 4B, that finally presents the structural information in the form of 3D stereo images. The focus of the 3D visualization is to obtain the 3D coordinates of each node and the correspondence between the eight nodes adjacent to the self-body elements. Subsequently, the 3D visualization model is established in combination with the reconstruction module in the software. The different groups of the image are segmented in grayscale, and each group is identified by color rendering. Figure 4C shows the 3D model of the pore of the CTB.

2.4.2 Pores and cracks segmentation

Porosity is the percentage of pore volume per unit volume, an essential index of the mesoscopic characteristics of the CTB. Based on the segmentation module of the software (ImageJ is accessible by the National Institutes of Health), the fast watershed algorithm was used to identify the boundaries of the CTB pores and calculate the area of the pores. Similarly, pore and crack volumes are obtained in this way. First, adjust the lowest gray value of the image to 0 and select the whole image, as shown in Figure 5A; Figure 5B is obtained after the gray value is adjusted and the pore and crack part is selected. To ensure the consistency of data processing, the same gray value is selected for all the cracks of CT samples after the SHPB test. The crack volume after impact is extracted by segmentation according to the difference between pore and crack volume.

3 Results and discussion

3.1 Initial pore distribution characteristic function of cemented tailings backfill

During each scan, the sample was rotated from 0° to 360° at increments of 0.49°/s, and a total set of 735 images projected on the detector screen was obtained after a full rotation. The dark patches at the top and bottom of the CT images of the CTB sample have a LOT of imaging artifacts. So, they were excluded from the analysis. From the statistics, it can be seen that the overall initial porosity distribution of CTB is stable. Figure 6 shows the porosity of each

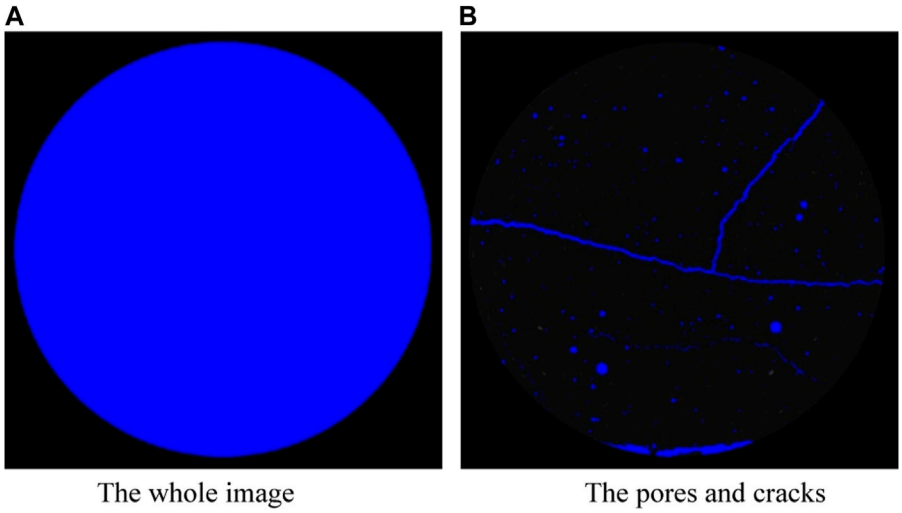

FIGURE 5
Pore and crack segmentation process.

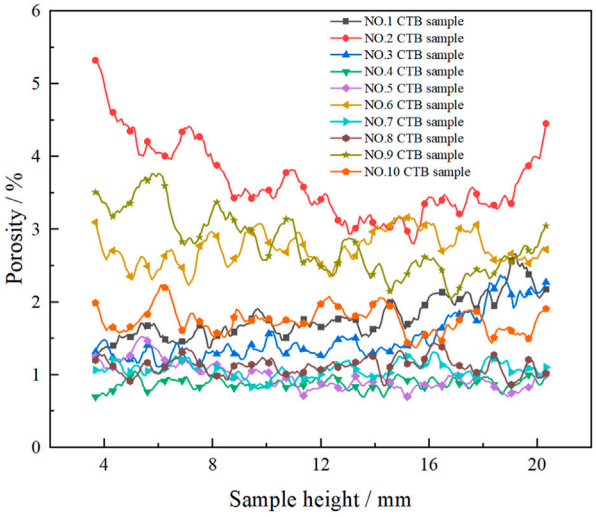

FIGURE 6
Relationship of CTB porosity with sample height.

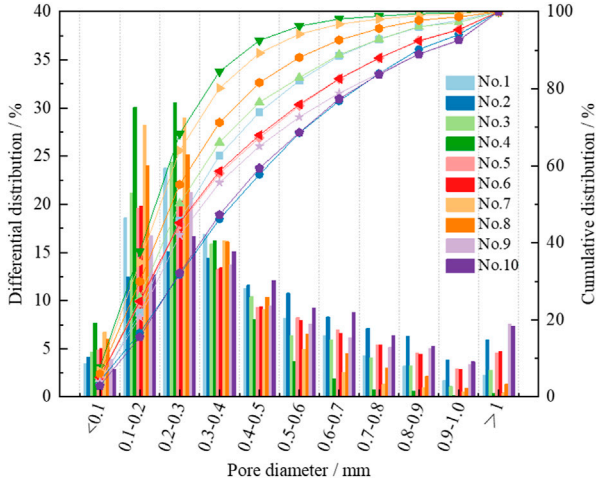

FIGURE 7
Pore diameter distribution of CTB.

image of the ten CTB samples. The porosity distribution of samples No. 4, 5, 7, and 8 is around 1%. The porosity of samples No. 1, 3, and 10 ranged from 1.2% to 2.4%, where the porosity of No. 10 was uniformly distributed with height, and the porosity of No. 1 and No. 3 became larger with height as a whole. The porosity of samples No. 6 and No. 9 is around 3%. No. 2 has the greatest variation in porosity, ranging from 3% to 5.4%.

3.2 Initial pore size analysis of cemented tailings backfill

Based on the analysis of the CT results of the CTB samples and the identification of their pore data according to the fast watershed algorithm, the statistical table of their pore sizes can be obtained. The pore size data are statistically analyzed to divide the pore sizes into ten intervals in the range of 0.2–1 mm, and the pore size distribution of the CTB samples is plotted in Figure 7.

Figure 7 shows the pore size distribution of the 10 CTB samples. The number of pores with sizes between 0.1 and 0.2 mm, between 0.2 and 0.3 mm is the highest, with samples No. 4, 7, and 8 being particularly prominent, with their pores accounting for 60%, 57%, and 49% of the size of the pores, respectively. The pores with the minuscule percentage are 0.9–1.0 mm, and only 0.5% and 0.8% of samples No. 7 and No. 8 pores are in this range. Pores smaller than 0.2 mm accounted for more than 40% of each sample. Samples No. 3 and 7 have more than 90% of pores with pore sizes less than 0.5 mm. The CTB contains many initial pores, and the pore size distribution characteristics are similar.

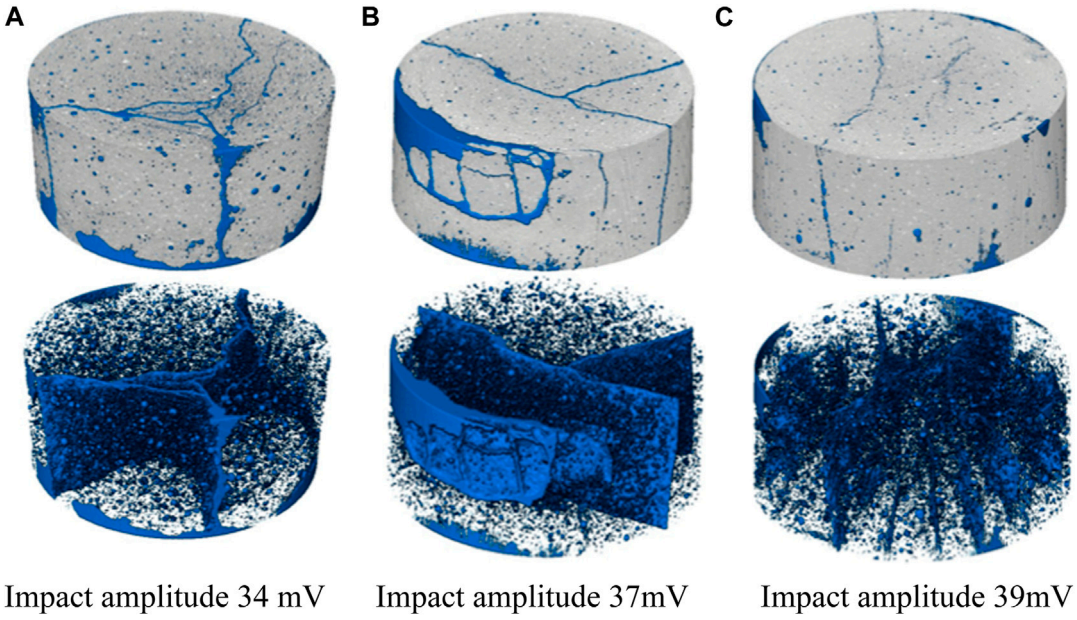

FIGURE 8
3D reconfiguration of CTB under low strain rate impact.

3.3 Crack volume analysis of cemented tailings backfill under low impact amplitude

Due to the limitation of the SHPB test, the minimum impact amplitude that the oscilloscope can collect is around 35 mV. The SHPB test with impact amplitudes of 34, 37, and 39 mV was carried out to observe the crack morphology of the CTB under the low strain rate impact, and the 3D reconstruction of the CTB under three impact amplitudes was obtained, as shown in Figure 6. For each set of the impact test, three parallel tests have been done and only one CTB sample after the impact test was selected for the CT test. The main reason for doing that is even though the recipe of the CTB samples is the same and they were prepared in the same batch, the failure pattern of the CTB samples differs, and some of them fail into small pieces after the impact test. We selected the more intact and complected sample (out of three parallel tests using the same impact amplitude) for the CT test.

From Figure 8, it can be observed that the crack pattern inside the CTB, when the impact amplitude is 34 mV, the CTB sample is mainly shear cracks, with occasional secondary cracks. When the impact amplitude was increased to 37 mV, the sample was damaged primarily by shear, with secondary cracks on the outer surface leading to small flakes. When the impact amplitude was further increased to 39 mV, it was apparent that the width of cracks became narrow, but the number of cracks increased. There were many secondary cracks around the major cracks. Fragments were falling off at the corners, the sample was further damaged, and the size of the fragment became smaller due to the increase in the number of cracks.

The crack volume can be obtained by the crack segmentation method in Section 2.4.2. The dynamic uniaxial compressive strength was obtained according to SHPB test. Figure 9 shows the relationship between impact amplitude, dynamic uniaxial compressive strength, and total crack volume of CTB. To further express the macroscopic morphology of the CTB cracks, we extracted the crack morphology of the specimens individually and represented it in Figure 9.

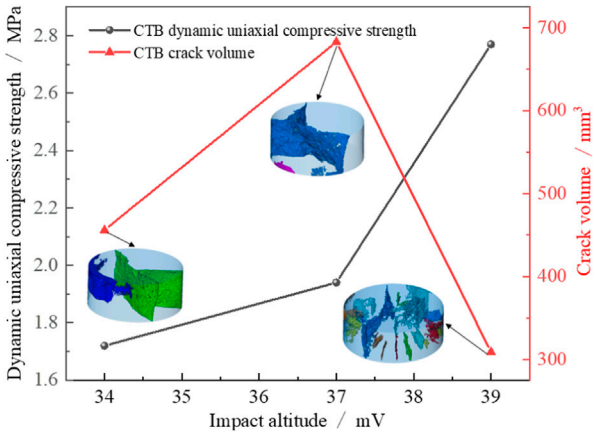

FIGURE 9
The relationship between the impact amplitude, the dynamic compressive strength, and the crack volume.

As shown in Figure 9, the dynamic compressive strength of CTB increased from 1.72 MPa to 2.77 MPa with the increase of impact amplitude, and the total volume of cracks produced after the SHPB test first increased and then decreased. When the impact amplitude was 34 mV, the gross volume of cracks was 456 mm^2. When the impact amplitude was 37 mV, the total volume of cracks was the largest, reaching 683 mm^3. When the impact amplitude was increased to 39 mV, the cracks' total volume was reduced to 309 mm^3. It can be seen in Figure 9 that the number of cracks increased when the impact amplitude was 39 mV. However, the

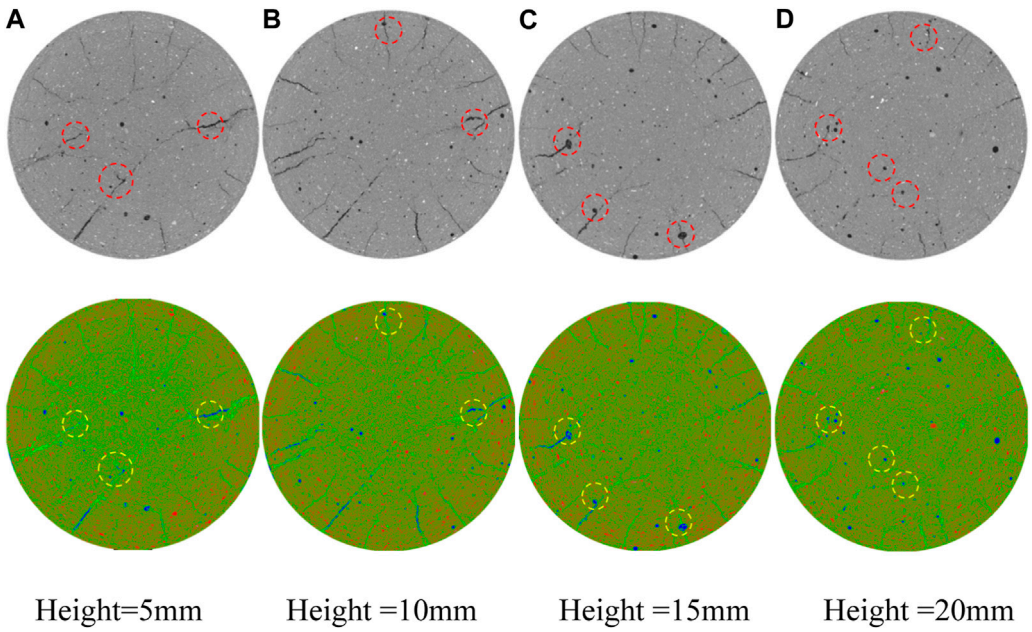

FIGURE 10
CT images of CTB samples at different heights after low strain rate impact test.

width and length of the cracks decrease, and therefore, the volume of each crack decreases.

Under the low strain rate impact, the damage of the CTB mainly exists in the form of shear cracks. As the impact amplitude increases, the dynamic compressive strength of the CTB increases, and the total volume of cracks produced by the post-impact damage first increases and then decreases, and the number of cracks increases.

3.4 Computerized tomography image analysis at the low impact amplitude of cemented tailings backfill

The slice images of the CTB were analyzed by uniformly extracting the 2D CT images of different heights, and sample NO. 3 with an impact amplitude of 39 mV was selected. Figure 10 shows the slice images of the CT sample at 5, 10, 15, and 20 mm.

The grayscale transform method converts a black-and-white image into a color image with a specific color distribution, facilitating better extraction of useful information from the image. The image enhancement effect is more evident if the gradation is finer and the color is more prosperous. The grayscale transform method converts the 2D CT image into a color image representing cracks, pores, and CTB. The blue part means defects such as pores and coarse cracks, the light green represents microcracks produced after SHPB tests, the red represents mineral crystals in the tailing sand, and the green represents the CTB.

From the analysis in Figure 10, it can be seen that the CTB samples contain apparent pores. Most of the cracks generated after impact are developed and expanded along the pores, indicating that when the CTB was subjected to impact loading, the stress concentration occurred in the space near the pores, which led to the development and further expansion of microcracks near the pores. With the increased impact amplitude, the microcracks develop into coarse cracks, further destabilizing the CTB structure.

4 Conclusion

In this paper, CT scanning tests were conducted on CTB samples before and after failure to study the microscopic properties and macroscopic mechanical correlation mechanisms of the CTB. The following conclusions were obtained.

(1) The dependence of the initial pore distribution of CTB with height was obtained. The overall initial porosity distribution of CTB is stable with the height. The porosity of most samples is between 1% and 2%. The number of pores with size between 0.1 and 0.3 mm is the largest.
(2) The dynamic uniaxial compressive strength of the CTB increased with impact amplitude. In the SHPB test with low impact amplitude, the total volume of cracks produced by post-impact first increased and then decreased, and the number of cracks increased as impact amplitude rose.
(3) The CTB contains an apparent pore structure. It is shown that when the CTB is subjected to impact loading, cracks mainly sprout and expand near the initial pores.

In this study, the research finding has revealed initial pore distribution characteristics and crack failure development of cemented tailings backfill under low impact amplitude. In future

work, the mechanical and mesoscopic features of host rock and CTB composite samples under low impact amplitude will be discussed. Additionally, the 3D-DIC techniques will be considered to observe the actual progress of the crack development of CTB in the SHPB tests.

Data availability statement

The raw data supporting the conclusion of this article will be made available by the authors, without undue reservation.

Author contributions

DZ: Data curation, Formal Analysis, Funding acquisition, Investigation, Methodology, Visualization, Writing–original draft, Writing–review and editing. GL: Funding acquisition, Resources, Supervision, Validation, Writing–original draft, Writing–review and editing. LG: Conceptualization, Funding acquisition, Supervision, Visualization, Writing–original draft, Writing–review and editing. XY: Funding acquisition, Investigation, Resources, Supervision, Writing–original draft, Writing–review and editing. SW: Supervision, Writing–original draft, Writing–review and editing. YZ: Funding acquisition, Supervision, Writing–original draft, Writing–review and editing.

Funding

The author(s) declare financial support was received for the research, authorship, and/or publication of this article. This research was funded by the National Key Research and Development Program of China, grant number Nos 2022YFC2904101, and the Beijing Nova Program, grant number Nos 20220484057 and 20230484242, the National Natural Science Foundation of China, grant number Nos 52274122 and 52204091, the Youth Science and Technology Innovation Fund of BGRIMM (04-2329), and the Exploration fund of BGRIMM (02-2229).

Acknowledgments

The authors also thank Professor Weidong Song and Professor Shuai Cao of the University of Science and Technology Beijing for their support and help in the test.

Conflict of interest

The authors declare that the research was conducted in the absence of any commercial or financial relationships that could be construed as a potential conflict of interest.

Publisher's note

References

Cao, S., Xue, G., Song, W., and Teng, Q. (2020). Strain rate effect on dynamic mechanical properties and microstructure of cemented tailings composites. *Constr. Build. Mat.* 247, 118537. doi:10.1016/j.conbuildmat.2020.118537

Chen, X., Shi, X., Zhou, J., Li, E., Qiu, P., and Gou, Y. (2021). High strain rate compressive strength behavior of cemented paste backfill using split Hopkinson pressure bar. *Int. J. Min. Sci. Technol.* 31, 387–399. doi:10.1016/j.ijmst.2021.03.008

Deng, X., Li, Y., Wang, F., Shi, X., Yang, Y., Xu, X., et al. (2022). Experimental study on the mechanical properties and consolidation mechanism of microbial grouted backfill. *Int. J. Min. Sci. Technol.*, 032–002. doi:10.1016/j.ijmst.2022.01.010

Dong, Y., Liao, Z., Wang, J., Liu, Q., and Cui, L. (2023). Potential failure patterns of a large landslide complex in the Three Gorges Reservoir area. *Bull. Eng. Geol. Environ.* 82 (1), 41. doi:10.1007/s10064-022-03062-7

Du, X., Feng, G., Zhang, M., Wang, Z., and Liu, W. (2022). Influence of backfilling rate on the stability of the "backfilling body-immediate roof" cooperative bearing structure. *Int. J. Min. Sci. Technol.* 32, 1197–1206. doi:10.1016/j.ijmst.2022.09.003

Emad, M. Z., Mitri, H., and Kelly, C. (2014). State-of-the-art review of backfill practices for sublevel stoping system. *Int. J. Surf. Min. Reclam. Environ.* 29, 544–556. doi:10.1080/17480930.2014.889363

Fang, K., Zhang, J., Tang, H., Hu, X., Yuan, H., Wang, X., et al. (2023). A quick and low-cost smartphone photogrammetry method for obtaining 3D particle size and shape. *Eng. Geol.* 322, 107170. doi:10.1016/j.enggeo.2023.107170

Gerges, N. N., Issa, C. A., and Fawaz, S. (2015). Effect of construction joints on the splitting tensile strength of concrete. *Case Stud. Constr. Mat.* 3, 83–91. doi:10.1016/j.cscm.2015.07.001

Ghasemi, S., Khamehchiyan, M., Taheri, A., Nikudel, M. R., and Zalooli, A. (2020). Crack evolution in damage stress thresholds in different minerals of granite rock. *Rock Mech. Rock Eng.* 53, 1163–1178. doi:10.1007/s00603-019-01964-9

Guggari, V. B., Kumar, H., and Budi, G. (2023). Numerical analysis for assessing the effects of crown pillar thickness on ore dilution around the sub-level open stopes. *Ain Shams Eng. J.*, 102301. doi:10.1016/j.asej.2023.102301

Guo, L., Liu, G., Ma, Q., and Chen, X. (2022). Research progress on mining with backfill technology of underground metalliferous mine. *Meitan Xuebao/Journal China Coal Soc.* 47, 4182–4200. doi:10.13225/j.cnki.jccs.2022.0720

Huang, Z., Cao, S., and Yilmaz, E. (2023). Microstructure and mechanical behavior of cemented gold/tungsten mine tailings-crushed rock backfill: effects of rock gradation and content. *J. Environ. Manage.* 339, 117897. doi:10.1016/j.jenvman.2023.117897

Jafari, M., Shahsavari, M., and Grabinsky, M. (2021). Drained triaxial compressive shear response of cemented paste backfill (CPB). *Rock Mech. Rock Eng.* 54, 3309–3325. doi:10.1007/s00603-021-02464-5

Kasap, T., Yilmaz, E., and Sari, M. (2022). Effects of mineral additives and age on microstructure evolution and durability properties of sand-reinforced cementitious mine backfills. *Constr. Build. Mat.* 352, 129079. doi:10.1016/j.conbuildmat.2022.129079

Li, G., Deng, G., and Ma, J. (2022). Numerical modelling of the response of cemented paste backfill under the blasting of an adjacent ore stope. *Constr. Build. Mater.* 343, 128051. doi:10.1016/j.conbuildmat.2022.128051

Li, J., Cao, S., and Song, W. (2023). Distribution development of pore/crack expansion and particle structure of cemented solid-waste composites based on CT and 3D reconstruction techniques. *Constr. Build. Mat.* 376, 130966. doi:10.1016/j.conbuildmat.2023.130966

Li, J., Yilmaz, E., and Cao, S. (2021). Influence of industrial solid waste as filling material on mechanical and microstructural characteristics of cementitious backfills. *Constr. Build. Mat.* 299, 124288. doi:10.1016/j.conbuildmat.2021.124288

Liu, L., Xin, J., Huan, C., Qi, C., Zhou, W., and Song, K. (2020). Pore and strength characteristics of cemented paste backfill using sulphide tailings: effect of sulphur content. *Constr. Build. Mat.* 237, 117452. doi:10.1016/j.conbuildmat.2019.117452

Liu, W., Pang, L., Liu, Y., and Du, Y. (2019). Characteristics analysis of roof overburden fracture in thick coal seam in deep mining and engineering application of super high water material in backfill mining. *Geotechnical Geol. Eng.* 37, 2485–2494. doi:10.1007/s10706-018-00770-4

Lu, H., Qi, C., Chen, Q., Gan, D., Xue, Z., and Hu, Y. (2018). A new procedure for recycling waste tailings as cemented paste backfill to underground stopes and open pits. *J. Clean. Prod.* 188, 601–612. doi:10.1016/j.jclepro.2018.04.041

Mohanto, S., and Deb, D. (2020). Prediction of plastic damage index for assessing rib pillar stability in underground metal mine using multi-variate regression and artificial neural network techniques. *Geotechnical Geol. Eng.* 38, 767–790. doi:10.1007/s10706-019-01065-y

Onederra, I. A., Furtney, J. K., Sellers, E., and Iverson, S. (2013). Modelling blast induced damage from a fully coupled explosive charge. *Int. J. Rock Mech. Min.* 58, 73–84. doi:10.1016/j.ijrmms.2012.10.004

Sarkar, G., and Siddiqua, S. (2016). Effect of fluid chemistry on the microstructure of light backfill: an X-ray CT investigation. *Eng. Geol.* 202, 153–162. doi:10.1016/j.enggeo.2016.01.012

Solismaa, S., Torppa, A., Kuva, J., Heikkilä, P., Hyvönen, S., Juntunen, P., et al. (2021). Substitution of cement with granulated blast furnace slag in cemented paste backfill: evaluation of technical and chemical properties. *Minerals* 11, 1068. doi:10.3390/min11101068

Sun, Q., Zhang, J., Zhang, Q., and Yan, H. (2018). A case study of mining-induced impacts on the stability of multi-tunnels with the backfill mining method and controlling strategies. *Environ. Earth Sci.* 77, 234. doi:10.1007/s12665-018-7414-6

Sun, W., Hou, K., Yang, Z., and Wen, Y. (2017). X-ray CT three-dimensional reconstruction and discrete element analysis of the cement paste backfill pore structure under uniaxial compression. *Constr. Build. Mat.* 138, 69–78. doi:10.1016/j.conbuildmat.2017.01.088

Sun, W., Zhang, S., Li, J., and Li, Z. (2022). Experimental study on energy dissipation of layered backfill under impact load. *Constr. Build. Mat.* 347, 128478. doi:10.1016/j.conbuildmat.2022.128478

Tan, Y., Wang, J., Song, W., Xu, L., and Cao, S. (2019). Experimental study on mechanical properties of cemented tailings backfill under cycle dynamic loading test. *Caikuang yu Anquan Gongcheng Xuebao/Journal Min. Saf. Eng.* 36, 184–190. doi:10.13545/j.cnki.jmse.2019.01.024

Tian, X., and Fall, M. (2021). Non-isothermal evolution of mechanical properties, pore structure and self-desiccation of cemented paste backfill. *Constr. Build. Mat.* 297, 123657. doi:10.1016/j.conbuildmat.2021.123657

Wang, A., Cao, S., and Yilmaz, E. (2022a). Effect of height to diameter ratio on dynamic characteristics of cemented tailings backfills with fiber reinforcement through impact loading. *Constr. Build. Mat.* 322, 126448. doi:10.1016/j.conbuildmat.2022.126448

Wang, J., Fu, J., Song, W., and Zhang, Y. (2022b). Effect of rice husk ash (RHA) dosage on pore structural and mechanical properties of cemented paste backfill. *J. Mater. Res. Technol.* 17, 840–851. doi:10.1016/j.jmrt.2022.01.044

Wang, R., Zeng, F., and Li, L. (2021). Stability analyses of side-exposed backfill considering mine depth and extraction of adjacent stope. *Int. J. Rock Mech. Min.* 142, 104735. doi:10.1016/j.ijrmms.2021.104735

Wang, Y., Liu, D., and Hu, Y. (2019). Monitoring of internal failure evolution in cemented paste backfill under uniaxial deformation using *in-situ* X-ray computed tomography. *Arab. J. Geosci.* 12, 138. doi:10.1007/s12517-019-4285-4

Wu, Q., Liu, Y., Tang, H., Kang, J., Wang, L., Li, C., et al. (2023). Experimental study of the influence of wetting and drying cycles on the strength of intact rock samples from a red stratum in the Three Gorges Reservoir area. *Eng. Geol.* 314, 107013. doi:10.1016/j.enggeo.2023.107013

Xia, K., Chen, C., Liu, X., Liu, X., Yuan, J., and Dang, S. (2023). Assessing the stability of high-level pillars in deeply-buried metal mines stabilized using cemented backfill. *Int. J. Rock Mech. Min.* 170, 105489. doi:10.1016/j.ijrmms.2023.105489

Xue, G., and Yilmaz, E. (2022). Strength, acoustic, and fractal behavior of fiber reinforced cemented tailings backfill subjected to triaxial compression loads. *Constr. Build. Mat.*, 338. doi:10.1016/j.conbuildmat.2022.127667

Xue, G., Yilmaz, E., Feng, G., Cao, S., and Sun, L. (2021). Reinforcement effect of polypropylene fiber on dynamic properties of cemented tailings backfill under SHPB impact loading. *Constr. Build. Mat.* 279, 122417. doi:10.1016/j.conbuildmat.2021.122417

Zhang, C., Wang, J., Song, W., and Fu, J. (2022). Pore structure, mechanical behavior and damage evolution of cemented paste backfill. *J. Mater. Res. Technol.* 17, 2864–2874. doi:10.1016/j.jmrt.2022.02.010

Zhang, C., Wang, J., Song, W., and Fu, J. (2023). Effect of waste glass powder on pore structure, mechanical properties and microstructure of cemented tailings backfill. *Constr. Build. Mat.* 365, 130062. doi:10.1016/j.conbuildmat.2022.130062

Zhang, Y., Wang, X., Wei, C., and Zhang, Q. (2017). Dynamic mechanical properties and instability behavior of layered backfill under intermediate strain rates. *Trans. nonferr. Metal. Soc.* 27, 1608–1617. doi:10.1016/S1003-6326(17)60183-3

Zheng, D., Song, W., Cao, S., and Li, J. (2022). Dynamical mechanical properties and microstructure characteristics of cemented tailings backfill considering coupled strain rates and confining pressures effects. *Constr. Build. Mat.* 320, 126321. doi:10.1016/j.conbuildmat.2022.126321

Zheng, D., Song, W., Cao, S., Li, J., and Sun, L. (2021). Investigation on dynamical mechanics, energy dissipation, and microstructural characteristics of cemented tailings backfill under SHPB tests. *Minerals* 11, 542. doi:10.3390/min11050542

Zhu, X., Guo, G., Zha, J., Chen, T., Fang, Q., and Yang, X. (2016). Surface dynamic subsidence prediction model of solid backfill mining. *Environ. Earth Sci.* 75, 1007. doi:10.1007/s12665-016-5817-9